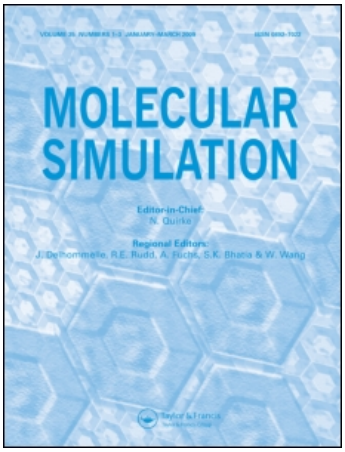

Molecular Simulation
Publication details, including instructions for authors and subscription information:
http://www.informaworld.com/smpp/title~content=t713644482

Gibbs Ensemble Monte Carlo Simulation of LJ Fluid in Cylindrical Pore with Energetically Heterogeneous Surface

Tatsuhiko Miyata[a]; Akira Endo[a]; Takuji Yamamoto[a]; Takao Ohmori[a]; Takaji Akiya[a]; Masaru Nakaiwa[a]
[a] Research Institute for Green Technology, National Institute of Advanced Industrial Science and Technology, Ibaraki, Japan

To cite this Article Miyata, Tatsuhiko , Endo, Akira , Yamamoto, Takuji , Ohmori, Takao , Akiya, Takaji and Nakaiwa, Masaru(2004) 'Gibbs Ensemble Monte Carlo Simulation of LJ Fluid in Cylindrical Pore with Energetically Heterogeneous Surface', Molecular Simulation, 30: 6, 353 — 359
To link to this Article: DOI: 10.1080/08927020310001645246
URL: http://dx.doi.org/10.1080/08927020310001645246

Molecular Simulation, Vol. 30 (6), 15 May 2004, pp. 353–359

Taylor & Francis
Taylor & Francis Group

Gibbs Ensemble Monte Carlo Simulation of LJ Fluid in Cylindrical Pore with Energetically Heterogeneous Surface

TATSUHIKO MIYATA*, AKIRA ENDO†, TAKUJI YAMAMOTO, TAKAO OHMORI, TAKAJI AKIYA and MASARU NAKAIWA

Research Institute for Green Technology, National Institute of Advanced Industrial Science and Technology, Tsukuba Central 5, 1-1-1, Higashi, Tsukuba, Ibaraki 305-8565, Japan

(Received May 2003; In final form October 2003)

The energetic heterogeneity effect of a solid surface on the phase behavior of a confined fluid within a narrow cylindrical pore was studied by means of Gibbs Ensemble Monte Carlo (GEMC) and canonical ensemble Monte Carlo (MC) simulations. The energetic heterogeneity was modeled as a local adsorbing site, and all the interactions considered were described by Lennard–Jones (LJ) potentials, i.e. 12–6 and 9–3 type. From the changes in the apparent shapes of isotherms, energetic heterogeneity on the solid surface was found to smear the phase transition region. The energetic heterogeneity of the solid internal surface causes an additive effect to pull the fluid particles toward the solid surface in the entire relative pressure region, leading to higher packing of the fluid particle layered in the vicinity of the pore wall compared with the homogeneous surface case at the same mean fluid density within the pore.

Keywords: Monte Carlo simulation; Lennard–Jones potentials; Isotherm and mean density; Energetic heterogeneity effect

INTRODUCTION

The influence of energetic heterogeneities of surface on adsorption is a long-standing problem in surface science. Much interest has been paid to the effect of surface heterogeneities on phase transitions of adsorbates [1–17]. For instance, impurities located on the surfaces were found to destroy the layering transition of adsorbates, and it was also pointed out that those impurities might cause new transitions [12].

In studying the effect of solid surface heterogeneity on adsorption, it is important to systematically examine adsorption isotherms, density profiles and thermodynamic quantities. Density profiles offer basic information for studying the phase behavior in terms of the fluid structure. The decomposition of the usual thermodynamic quantities such as internal energy into more elemental components will provide helpful information in discussing phase behavior in terms of thermodynamics. The concept of this decomposition itself was previously used by Bojan and Steele [2,3,8].

In the theoretical studies dealing with energetically heterogeneous solid surfaces, geometries of a single plane surface and slit-like pore have been used to examine properties of adsorbed layers and phase transition phenomena of inhomogeneous fluids [5–7,9–13,16]. In particular, Patrykiejew and coworkers have intensively studied the behaviors observed in the region from sub-monolayer to multilayer, including the phase transitions such as prewetting–wetting transition and layering transition [5–7,9–13]. However, for the phase transition associated with capillary condensation, there seem to be no systematic studies that focus on the thermodynamic quantities of confined fluids in a narrow pore with an energetically heterogeneous internal surface, especially in both the case that the surface is significantly curved and that the decomposition analysis of the internal energy into elemental components is applied.

We examined the energetic heterogeneity effect of the surface on the phase behavior of the fluids confined in a cylindrical pore by means of Monte Carlo (MC) simulation. Note that a cylindrical pore is one of the useful geometries in modeling the pore

*Present address: Department of Theoretical Studies, Institute for Molecular Science, 38, Nishigo-Naka, Myodaiji, Okazaki, Aichi 444-8585, Japan.
†Corresponding author. Tel.: +81-29-861-4653. Fax: +81-29-861-4660. E-mail: endo-akira@aist.go.jp

ISSN 0892-7022 print/ISSN 1029-0435 online © 2004 Taylor & Francis Ltd
DOI: 10.1080/08927020310001645246

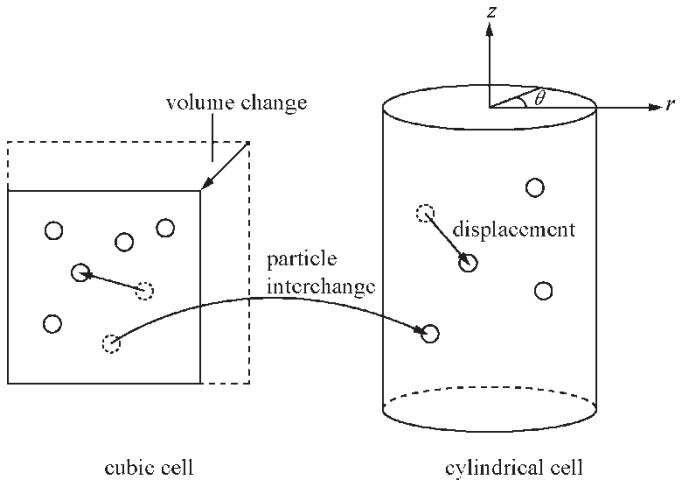

FIGURE 1 Schematic representation of two unit cells used in the GEMC simulation.

of real porous materials (see, e.g. Refs. [18,19]). Both the Gibbs ensemble (GE) and the NVT ensemble were used to reduce the total CPU time without losing accuracies in ensemble averages. All the interaction models we used were the Lennard–Jones (LJ) potentials.

COMPUTATIONAL DETAILS

Interaction Model

A cubic and a cylindrical unit cell were used in the Gibbs Ensemble Monte Carlo (GEMC) simulations (Fig. 1). The coordinates in the cylindrical cell (r, θ, z) are shown in Fig. 1. The unit cell length in z direction of the cylindrical cell, L_{pore}, was $L_{\text{pore}}/\sigma_{\text{FF}} = 30$, where σ_{FF} is the core diameter of the fluid particle. The periodic boundary conditions were applied in all directions for the cubic cell, whereas only in z direction for the cylindrical cell.

For the fluid–fluid interaction, the LJ 12–6 potential was used as

$$\phi_{\text{FF}}(r_{\text{pair}}) = 4\varepsilon_{\text{FF}}\left[\left(\frac{\sigma_{\text{FF}}}{r_{\text{pair}}}\right)^{12} - \left(\frac{\sigma_{\text{FF}}}{r_{\text{pair}}}\right)^{6}\right], \qquad (1)$$

where ϕ_{FF}, r_{pair} and ε_{FF} are the fluid–fluid pair potential, molecular separation and the energy parameter, respectively. ϕ_{FF} was cut off at $5\sigma_{\text{FF}}$.

The wall–fluid interaction, ϕ_{WF}, was given by

$$\phi_{\text{WF}} = \phi_{\text{SF}} + \phi_{\text{LF}}, \qquad (2)$$

where ϕ_{SF} and ϕ_{LF} represent the interaction between solid matrix–fluid particle and that between local adsorbing site–fluid particle, respectively. The solid matrix was assumed to be atomically structureless. The pore diameter $d_{\text{pore}}/\sigma_{\text{FF}} = 10$ was used entirely. The local adsorbing sites were responsible for the energetic heterogeneities on the internal surface of the pore, and if there were no such sites, then the internal surface was regarded to be homogeneous. The local adsorbing sites were assumed to be immobile and located randomly so that the coordinates of these sites in the radial direction were equal to $d_{\text{pore}}/2$. In putting these sites on the surface, the central distances between any of two sites were separated at least σ_{LL}, where σ_{LL} is the core diameter of the sites, to avoid a significant overlap of these sites. $\sigma_{\text{LL}}/\sigma_{\text{FF}} = 1$ was employed entirely. For ϕ_{SF}, the shifted LJ 9–3 potential was used as

$$\phi_{\text{SF}}(r) = 4\varepsilon_{\text{SF}}\left[\left(\frac{\sigma_{\text{SF}}}{d_{\text{pore}}/2 - r}\right)^{9} - \left(\frac{\sigma_{\text{SF}}}{d_{\text{pore}}/2 - r}\right)^{3} + C\right], \qquad (3)$$

where ε_{SF}, σ_{SF} and C are parameters in the potential. In this study, three sets of (ε_{SF}, σ_{SF}, C) were used as

TABLE I Models of solid surface and corresponding parameters

Model solid	$\varepsilon_{SF}/\varepsilon_{FF}$	σ_{SF}/σ_{FF}	C	$\rho_s\sigma_{FF}^3$	$\varepsilon_{LF}/\varepsilon_{FF}$	$N_L\sigma_{FF}^2/(\pi d_{pore}L_{pore})$
Solid A	6.569	0.7115	− 0.06996	1.0	–	0
Solid B	7.896	0.7117	− 0.08323	1.2	–	0
Solid C	9.224	0.7118	− 0.09646	1.4	–	0
Solid D	6.569	0.7115	− 0.06996	1.0	1.0	0.2493
Solid E	6.569	0.7115	− 0.06996	1.0	1.0	0.6791
Solid F	6.569	0.7115	− 0.06996	1.0	2.0	0.1061
Solid G	6.569	0.7115	− 0.06996	1.0	2.0	0.3395

"Solid A, B and C", respectively (Table I). In the order from "Solid A" to "Solid C", the interaction between solid matrix and fluid particle is strengthened. The parameter set of "Solid A" was used also for the simulations of the energetically heterogeneous solid surfaces, as summarized in Table I (from "Solid D" to "Solid G"). "Solid B and C" were used only for the simulations of homogeneous surfaces. With Eq. (3) these parameters reproduce the following equation well with $\varepsilon'_{SF}/\varepsilon_{FF} = \sigma'_{SF}/\sigma_{FF} = 1$ and the corresponding ρ_S shown in Table I:

$$\phi_{SF}(r) = \pi\varepsilon'_{SF}\rho_S\left[\frac{7\sigma'^{12}_{SF}}{32}K_9(r) - \sigma'^{6}_{SF}K_3(r)\right], \quad (4)$$

where

$$K_n(r) = \left(\frac{d_{pore}}{2}\right)^{-n}\int_0^{\pi} d\theta\left\{-\frac{2r}{d_{pore}}\cos\theta + \left[1-\left(\frac{2r}{d_{pore}}\right)^2\sin^2\theta\right]^{1/2}\right\}^{-n}. \quad (5)$$

Here, ρ_S is the number density of the LJ particle constituting the solid matrix, and ε'_{SF} and σ'_{SF} are parameters in the potential. Equation (4) is derived by the integration of the LJ 12–6 potential over the solid matrix [20]. For ϕ_{LF}, the LJ 12–6 potential

$$\phi_{LF}(r_{pair}) = 4\varepsilon_{LF}\left[\left(\frac{\sigma_{LF}}{r_{pair}}\right)^{12} - \left(\frac{\sigma_{LF}}{r_{pair}}\right)^{6}\right] \quad (6)$$

was used, where ε_{LF} and σ_{LF} are the parameters in the potential. The ϕ_{LF} was cut off at $5\sigma_{LF}$. The parameter sets of $(\varepsilon_{LF}/\varepsilon_{FF}, \sigma_{LF}/\sigma_{FF}) = (1, 1)$ and $(2, 1)$ were used. The σ_{LF} was given by $(\sigma_{FF} + \sigma_{LL})/2$ as usual. Variety of energetic heterogeneities were described by different surface densities of local adsorbing sites (Table I). Here, $N_L\sigma^2_{FF}/(\pi d_{pore}L_{pore})$ represents the surface density of the local adsorbing site, and N_L the number of local sites given in the cylindrical unit cell.

Simulation Methods

The phase coexistence between bulk fluid and confined fluid can be simulated by the GEMC method [21–25]. In our study, the GEMC method of keeping the pressure of bulk fluid constant [24,25] was employed. One MC cycle consisted of N_p displacement attempts, $6N_p$ particle interchange attempts and 1 volume change attempt, where N_p represents the total number of fluid particles.

The temperature, k_BT/ε_{FF}, was kept constant at 1.2 herein, which is slightly below the critical temperature 1.32 [26], where k_B is the Boltzmann constant. The number density, ρ, converged within 1000 MC cycles in our simulations. 5000 MC cycles were performed including the initial equilibration of 2000 MC cycles. ρ is defined by

$$\rho_b = \frac{\langle N_{p,b}\rangle}{\langle V_b\rangle} \quad (7)$$

$$\rho_c = \frac{\langle N_{p,c}\rangle}{V_c} = \frac{4\langle N_{p,c}\rangle}{\pi d^2_{pore}L_{pore}} \quad (8)$$

where V represents the volume of cell. Subscripts "b" and "c" stand for bulk fluid and confined fluid, respectively, and the bracket represents the ensemble average. The fluid particles above 2000 in number were considered in the GEMC simulations.

After the corresponding GEMC simulation run, the obtained mean number of the confined fluid particles were used in the following NVT–MC simulations of the confined fluid. From the NVT–MC simulations of confined fluids, the spatial density fluctuation, the accessible pore volumes for the fluid particles, the internal energy and its elemental components were evaluated. The aim of evaluating the accessible pore volumes, V_{access}, for the particle bodies of the confined fluid is to estimate a more precise mean density, $\rho_{c,access}$, of the confined fluid than ρ_c. Since V_c involves the dead volume for the fluid particles which comes from the excluded volumes of the most outer molecules constituting the solid matrix, ρ_c becomes smaller than $\rho_{c,access}$. The evaluation procedure of V_{access} was as follows: after evaluating the spatial density fluctuation in the corresponding NVT–MC simulation, one point was randomly chosen in the cylindrical cell. Then, we examined all the pre-evaluated density values within the sphere of diameter σ_{FF} whose center was located at the chosen point. If all the pre-evaluated density values were zero within the sphere, then the chosen point was regarded as inaccessible for the fluid particle body, i.e. this trial failed to find an accessible point in the cylindrical cell. If not, then the chosen point was regarded as accessible, i.e. succeeded in finding an accessible point. After repeating this procedure N_{trial} times, the accessible pore volume, V_{access}, was evaluated as

$$V_{access} = \frac{N_{success}}{N_{trial}}V_c = \frac{\pi d^2_{pore}L_{pore}N_{success}}{4N_{trial}}, \quad (9)$$

where $N_{success}$ represents the number of trials succeeded in finding an accessible point. In Eq. (9), $N_{trial} = 10^6$ was used. The confined fluid density, $\rho_{c,access}$, is defined by

$$\rho_{c,access} = \frac{N_{p,c}}{V_{access}}. \quad (10)$$

Under the assumption of the pairwise additivity [27], the internal energy, e_c, of confined fluids within a pore can be decomposed into three elemental components, i.e.

$$e_c = \langle k \rangle + \langle u_{c,FF} \rangle + \langle u_{c,WF} \rangle$$
$$= \frac{3}{2} k_B T + \langle u_{c,FF} \rangle + \langle u_{c,WF} \rangle, \quad (11)$$

where k, $u_{c,FF}$ and $u_{c,WF}$ represent kinetic energy, fluid–fluid interaction energy and wall–fluid interaction energy, respectively. Here, thermodynamic quantities are given as those per one molecule. $\langle u_{c,FF} \rangle$ and $\langle u_{c,WF} \rangle$ were evaluated simply as

$$\langle u_{c,FF} \rangle = \frac{1}{N_{p,c}} \left\langle \sum_i \sum_{j>i} \phi_{FF}(\mathbf{r}_i, \mathbf{r}_j) \right\rangle \quad (12)$$

$$\langle u_{c,WF} \rangle = \frac{1}{N_{p,c}} \left\langle \sum_i \phi_{WF}(\mathbf{r}_i) \right\rangle$$
$$= \frac{1}{N_{p,c}} \left\langle \sum_i \phi_{SF}(\mathbf{r}_i) \right\rangle + \frac{1}{N_{p,c}} \left\langle \sum_i \phi_{LF}(\mathbf{r}_i) \right\rangle, \quad (13)$$

where $\mathbf{r}_i$ ($\mathbf{r}_j$) represents the position vector of ith (jth) fluid particle. Two terms in the right hand side of Eq. (13) correspond to $\langle u_{c,SF} \rangle$ and $\langle u_{c,LF} \rangle$, respectively, where $u_{c,SF}$ and $u_{c,LF}$ represent solid matrix–fluid particle interaction energy and local adsorbing site–fluid particle interaction energy, respectively.

RESULTS AND DISCUSSION

Isotherm and Mean Density

Since the changes in V_{access} along the adsorption isotherm are in practice negligible (within 1%), the value of $\rho_{c,access}\sigma_{FF}^3$, evaluated by Eq. (10), will be used as the adsorbed amount in the adsorption isotherm in the following context. Figure 2 shows the adsorption isotherms in the cylindrical pore both with energetically homogeneous, i.e. atomically structureless internal surface and with energetically heterogeneous one. The lateral axis in Fig. 2 indicates the relative pressure P/P_0, where P and P_0 represent the pressure of the bulk gaseous fluid applied in the GEMC simulation and the saturation vapor pressure, respectively. P_0 was evaluated from the independent GEMC simulation with two cubic cells as $P_0\sigma_{FF}^3/\varepsilon = 0.0804$ when $k_BT/\varepsilon = 1.2$. As P/P_0 increases, one can find the region where the adsorbed amounts abruptly increase, especially when the surface density of local adsorbing site is small. This corresponds to the apparent phase transition region. The density of the bulk liquid state equilibrated with its vapor at $k_BT/\varepsilon = 1.2$ is also shown in Fig. 2 by a horizontal line, for comparison. Concerning

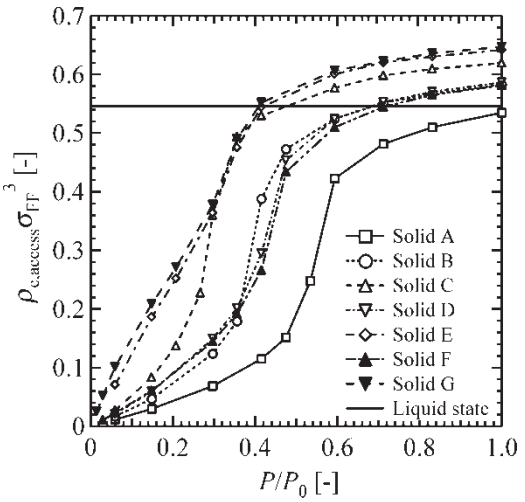

FIGURE 2 Adsorption isotherms represented by $\rho_{c,access}\sigma_{FF}^3$.

the energetically homogeneous internal surface, as the solid matrix–fluid particle interaction is strengthened (i.e. from "Solid A" to "Solid C"), the mean densities of the confined fluids increase in the whole region of the relative pressure. Similarly, as for the energetically heterogeneous surface, the mean densities of the confined fluids increase in the whole relative pressure region with increasing the surface density of the local adsorbing site, because the total wall–fluid interaction is strengthened by increasing the surface density of the local adsorbing site. The apparent phase transition region also shifts to the lower relative pressure region, i.e. lower chemical potential region. On the shapes of isotherms, we shall point out that the energetic heterogeneities on the solid internal surface modeled by local adsorbing sites tend to smear the apparent phase transition region. This tendency is remarkable in "Solid E" and "Solid G". Similar results were also reported for the slit-like pore by Gac *et al.* [13]. Above the pressures where the mean densities abruptly increase, all the mean densities of the confined fluids seem to be close to that of the bulk liquid state, indicating that the confined fluid is in the fully condensed liquid-like state after the completion of pore filling. The changes in mean fluid density mentioned above imply that the thermodynamic states of the confined fluids in the pore are significantly changed by the strength of the solid–fluid particle interaction.

Spatial Density Fluctuation and Thermodynamic Quantities

This section examines the spatial density fluctuations and thermodynamic quantities. The confined fluid in the pore is homogeneous in the directions of θ and z in atomically structureless surface cases, while in energetically heterogeneous surface cases, the confined fluid is structured in all three directions

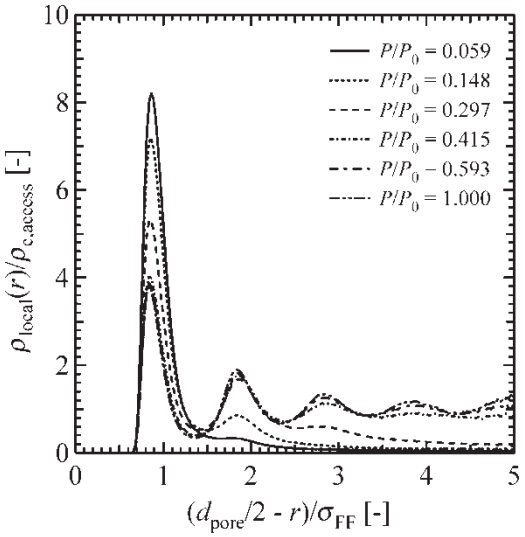

FIGURE 3 An example of the spatial density fluctuation within "Solid G".

due to the local adsorbing site–fluid particle interaction, $\phi_{LF}(r, \theta, z)$, in addition to the solid matrix–fluid particle interaction, $\phi_{SF}(r)$. In the analysis of spatial density fluctuations, the fluid structures only in the direction of r are focused, where the density fluctuations in the directions of θ and z are averaged. Figure 3 shows an example of the spatial density fluctuation of the confined fluid ("Solid G") along the isotherm, where density profiles are represented in the normalized form by $\rho_{c,access}$. The phase transition point of "Solid G" associated with the capillary condensation is approximately $P/P_0 = 0.3$ (Fig. 2). When $P/P_0 < 0.3$, fluid particles form condensed layers close to the pore wall and the densities near the center of pore are quite low, namely liquid-like "film" state. When $P/P_0 > 0.3$, fluid densities at the center of pore take close value to $\rho_{c,access}$ due to the completion of the pore filling, namely fully condensed liquid-like state. It is found that when $P/P_0 > 0.3$, the fluid has a significant structure with five layers including the most inner layer.

To discuss the smearing of phase transition from a viewpoint of fluid structure, we calculate the mean densities in each layer of confined fluids by

$$\overline{\rho}_{layer} = \frac{1}{\pi\left(r_{upper}^2 - r_{lower}^2\right)} \int_{r_{lower}}^{r_{upper}} 2\pi r \rho_{local}(r) dr, \quad (14)$$

where $\overline{\rho}_{layer}$, $\rho_{local}(r)$ and $r_{lower}(r_{upper})$ represent the mean density of the layer, density profile, the lower (upper) border of the layer in the direction of r, respectively. Here, r_{lower} and r_{upper} were defined as the radial positions where $\rho_{local}(r)$ took local minimum values. In the cases of liquid-like "film" state, only the layers that possess two definite borders are considered. Table II shows typical values of $\overline{\rho}_{layer}$ normalized by $\rho_{c,access}$, where the layers are labeled so that those closest to the pore wall are 1 and those most inner in the pore are 5. Overall, the values of $\overline{\rho}_{layer}/\rho_{c,access}$ in the first layer decrease with an increase in the relative pressure, whereas those in the inner four layers from second to fifth increase. The gradual decrease of $\overline{\rho}_{layer}/\rho_{c,access}$ in the first layer with increasing P/P_0 is attributed to the gradual growth of the inner layer. Here, we divide the dependence of $\overline{\rho}_{layer}/\rho_{c,access}$ on P/P_0 into two parts according to the phase transition pressure, i.e. the fully condensed liquid-like state and the liquid-like

TABLE II Mean density in each layer of confined fluids. The notations in the parenthesis, "film", "tran", and "fully", stand for the liquid-like "film" state, phase "transition" region, and "fully" condensed liquid-like state, respectively

	$P/P_0[-]$	$\overline{\rho}_{layer}/\rho_{c,access}[-]$				
		Layer 1	*Layer 2*	*Layer 3*	*Layer 4*	*Layer 5*
Solid A	0.297 (film)	1.80				
	0.415 (film)	1.70				
	0.593 (fully)	1.19	1.13	1.18	1.20	1.20
	1.00 (fully)	1.24	1.13	1.18	1.21	1.21
Solid C	0.148 (film)	2.16				
	0.297 (tran)	1.59	1.09			
	0.415 (fully)	1.35	1.10	1.09	1.11	1.10
	0.593 (fully)	1.34	1.10	1.11	1.12	1.11
	1.00 (fully)	1.37	1.09	1.10	1.12	1.11
Solid F	0.059 (film)	2.52				
	0.148 (film)	2.66				
	0.297 (tran)	2.09	0.99			
	0.415 (fully)	1.57	1.01	0.94	0.85	0.82
	0.593 (fully)	1.51	1.05	0.98	0.97	0.96
	1.00 (fully)	1.44	1.03	1.02	1.02	1.00
Solid G	0.148 (film)	2.11				
	0.297 (tran)	1.78	1.01			
	0.415 (fully)	1.48	1.08	1.03	1.00	0.97
	0.593 (fully)	1.33	1.09	1.10	1.10	1.10
	1.00 (fully)	1.32	1.10	1.11	1.12	1.12

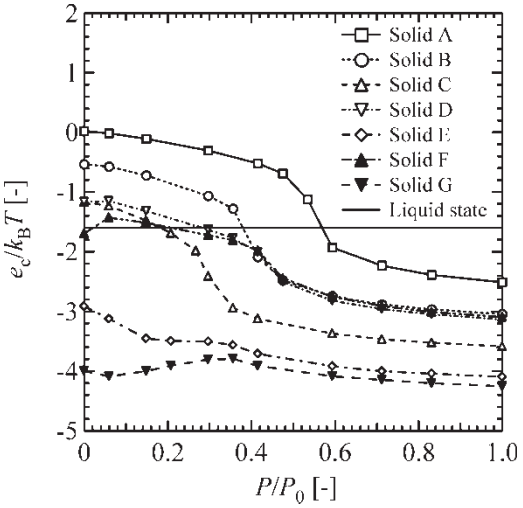

FIGURE 4 Dependence of the internal energy of confined fluid, e_c, on relative pressure, P/P_0.

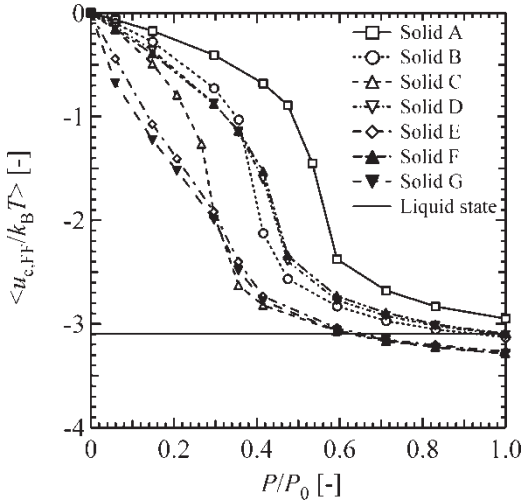

FIGURE 5 Dependence of $\langle u_{c,FF}\rangle$ on relative pressure, P/P_0.

"film" state. The states of the confined fluids are also indicated in Table II. In the case of energetically homogeneous surfaces of "Solid A" and "Solid C", the mean density in each layer, $\overline{\rho}_{layer}/\rho_{c,access}$, is almost constant when the confined fluid is in the fully condensed liquid-like state, and the gradual decrease of $\overline{\rho}_{layer}/\rho_{c,access}$ in the first layer with increasing P/P_0 is observed only in the liquid-like "film" state when the relative pressure is lower than the phase transition point. Thus, in regard to the energetically homogeneous solid surfaces, the liquid-like "film" state is featured by the gradual decrease of $\overline{\rho}_{layer}/\rho_{c,access}$ in the first layer, whereas the fully condensed liquid-like state is characterized by a constant $\overline{\rho}_{layer}/\rho_{c,access}$ in each layer. On the other hand, regarding the energetically heterogeneous surfaces, $\overline{\rho}_{layer}/\rho_{c,access}$ in the first layer significantly decreases even in the fully condensed liquid-like state. Correspondingly, the values of $\overline{\rho}_{layer}/\rho_{c,access}$ in the inner four layers from second to fifth tend to increase throughout the entire region of P/P_0. This tendency is enhanced by increasing the surface density of local adsorbing site. For a quantitative comparison, we employ the data of "Solid C" and of "Solid G", whose isotherms agree fairly well at $P/P_0 \geq 0.297$, and the values of $\overline{\rho}_{layer}/\rho_{c,access}$ are compared. In the region of $P/P_0 \geq 0.297$, $\overline{\rho}_{layer}/\rho_{c,access}$ in the first layer for "Solid G" is remarkably higher than that for "Solid C" at each P/P_0. This tendency reflected in the lower values of $\overline{\rho}_{layer}/\rho_{c,access}$ in the inner four layers from second to fifth for "solid G" than those for "Solid C". This comparison demonstrates that the structure of the confined fluid in heterogeneous surface cases is significantly different from that in homogeneous surface cases even at the same mean densities of fluids. Hence, we conclude that the energetic heterogeneity on the solid surface modeled by local adsorbing sites causes the additive effect to pull the fluid particles toward the solid surface in the entire relative pressure, namely an "additive pulling effect". This effect further induces the smearing of the phase transition point through the extension of the feature in the liquid-like "film" state to the fully condensed liquid-like state, observed as a gradual decrease of $\overline{\rho}_{layer}/\rho_{c,access}$ in the first layer.

We examine several kinds of elemental components of the internal energy. Based on Eqs. (11)–(13), e_c, $\langle u_{c,FF}\rangle$, $\langle u_{c,WF}\rangle$, $\langle u_{c,LF}\rangle$ and $\langle u_{c,SF}\rangle$ were evaluated. The dependences of e_c, $\langle u_{c,FF}\rangle$ and $\langle u_{c,SF}\rangle$ on P/P_0 are representatively shown in Figs. 4–6, respectively. Both $\langle u_{c,WF}\rangle$ and $\langle u_{c,LF}\rangle$, which are not shown in the figures, have similar dependences on P/P_0 as that of $\langle u_{c,SF}\rangle$: while they increase significantly with increasing P/P_0 in the liquid-like "film" state, they have little dependence on P/P_0 in the fully

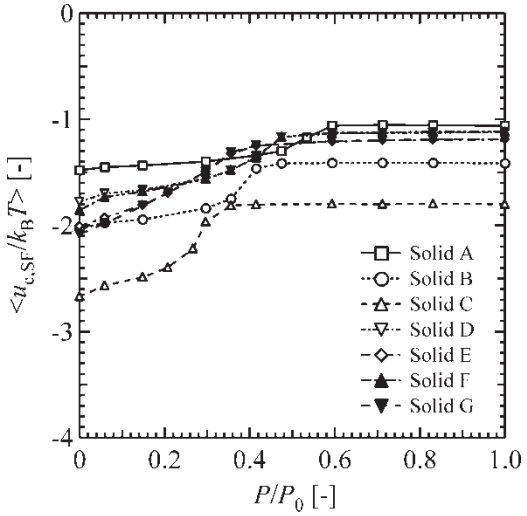

FIGURE 6 Dependence of $\langle u_{c,SF}\rangle$ on relative pressure, P/P_0.

condensed liquid-like state. The decomposed elemental components, $\langle u_{c,FF} \rangle$ and $\langle u_{c,WF} \rangle$, have opposite dependences on P/P_0: that is, $\langle u_{c,FF} \rangle$ decreases with P/P_0, whereas $\langle u_{c,WF} \rangle$ increases with P/P_0. These opposite dependences cancel out with each other in the overall internal energy, e_c, and especially in the heterogeneous surface cases, the dependence of e_c on P/P_0 is remarkably small compared with the homogeneous surface cases. These small dependences of e_c on P/P_0 can be associated with the smearing of the phase transition.

CONCLUSION

The energetic heterogeneity effect of a solid surface on the phase behavior of a confined fluid within a cylindrical pore was studied by means of GEMC and NVT–MC simulations The energetic heterogeneity was modeled by putting local adsorbing sites on solid internal surfaces. LJ potentials were used entirely. Adsorption isotherms, spatial density fluctuations, internal energy and its decomposed elemental components were evaluated. The main findings obtained were as follows: (1) The energetic heterogeneity of surfaces tends to smear the phase transition. (2) The energetic heterogeneity of the solid surface causes the additive effect to pull the fluid particles toward the solid surface in the entire relative pressure region, namely "additive pulling effect". This effect heightens the mean density in the layer closest to the pore wall even in the fully condensed liquid-like state, and is associated with the "smearing" of the phase transition. In the cases of energetically homogeneous surfaces, no such "additive pulling effect" is observed in the fully condensed liquid-like state.

References

[1] Bojan, M.J. and Steele, W.A. (1988) "Computer simulation of physisorption on a heterogeneous surface", *Surf. Sci.* **199**, L395–L402.

[2] Bojan, M.J. and Steele, W.A. (1989) "Computer simulation of physisorbed Kr on a heterogeneous surface", *Langmuir* **5**, 625–633.

[3] Steele, W.A. and Bojan, M.J. (1989) "Computer simulation studies of the heats of adsorption of simple gases", *Pure Appl. Chem.* **61**, 1927–1932.

[4] Albano, E.V., Binder, K., Heermann, D.W. and Paul, W. (1989) "Adsorption on stepped surfaces: a Monte Carlo simulation", *Surf. Sci.* **223**, 151–178.

[5] Patrykiejew, A. (1992) "Monte Carlo studies of adsorption III: localized monolayers on randomly heterogeneous surfaces", *Thin Solid Films* **208**, 189–196.

[6] Patrykiejew, A. (1993) "Monte Carlo studies of adsorption IV: phase transitions in localized monolayers on patchwise heterogeneous surfaces", *Thin Solid Films* **223**, 39–50.

[7] Patrykiejew, A. (1993) "Monte Carlo study of adsorption on heterogeneous surfaces: finite size and boundary effects in localized monolayers", *Langmuir* **9**, 2562–2568.

[8] Bojan, M.J. and Steele, W.A. (1993) "Computer simulation of physical adsorption on stepped surfaces", *Langmuir* **9**, 2569–2575.

[9] Chmiel, G., Patrykiejew, A., Rżysko, W. and Sokołowski, S. (1993) "Influence of surface energetic heterogeneity on the formation of adsorbed layers and wetting of solid surfaces: a Monte Carlo study", *Phys. Rev. B* **48**, 14454–14462.

[10] Gac, W., Patrykiejew, A. and Sokołowski, S. (1994) "Influence of surface energetical heterogeneity on capillary condensation in slit-like pores: a Monte Carlo study", *Surf. Sci.* **306**, 434–446.

[11] Gac, W., Patrykiejew, A. and Sokołowski, S. (1994) "Effects of random quenched impurities on wetting of solids: a Monte Carlo study", *Surf. Sci.* **318**, 413–420.

[12] Gac, W., Kruk, M., Patrykiejew, A. and Sokołowski, S. (1996) "Effects of random quenched impurities on layering transitions: a Monte Carlo study", *Langmuir* **12**, 159–169.

[13] Gac, W., Patrykiejew, A. and Sokołowski, S. (1997) "Monte Carlo study of adsorption in energetically and geometrically nonuniform slit-like pores", *Thin Solid Films* **298**, 22–32.

[14] Galle, J., Vörtler, H.L. and Schneider, K.P. (1997) "Monte Carlo simulation of hard sphere fluids in planar slits with molecularly rough surfaces", *Surf. Sci.* **387**, 78–85.

[15] Bryk, P., Henderson, D. and Sokołowski, S. (1999) "The wetting transition associated with the adsorption of a gas on a rough surface", *Langmuir* **15**, 6026–6034.

[16] Rżysko, W., Pizio, O., Sokołowski, S. and Sokołowska, Z. (1999) "Application of the replica Ornstein-Zernike equations to study submonolayer adsorption on energetically heterogeneous surfaces", *J. Colloid Interface Sci.* **219**, 184–189.

[17] Diestler, D.J. and Schoen, M. (2000) "Correlation of stress and structure in a simple fluid confined to a pore with furrowed walls", *Phys. Rev. E* **62**, 6615–6627.

[18] Neimark, A.V. and Ravikovitch, P.I. (2001) "Capillary condensation in MMS and pore structure characterization", *Micropor. Mesopor. Mat.* **44**, 697–707.

[19] Miyata, T., Endo, A., Ohmori, T., Akiya, T. and Nakaiwa, M. (2003) "Evaluation of pore size distribution in boundary region of micropore and mesopore using gas adsorption method", *J. Colloid Interface Sci.*, In press.

[20] Peterson, B.K., Walton, J.P.R.B. and Gubbins, K.E. (1986) "Fluid behaviour in narrow pores", *J. Chem. Soc. Faraday Trans. II* **82**, 1789–1800.

[21] Panagiotopoulos, A.Z. (1987) "Direct determination of phase coexistence properties of fluids by Monte Carlo simulation in a new ensemble", *Mol. Phys.* **61**, 813–826.

[22] Panagiotopoulos, A.Z. (1987) "Adsorption and capillary condensation of fluids in cylindrical pores by Monte Carlo simulation in the Gibbs ensemble", *Mol. Phys.* **62**, 701–719.

[23] Panagiotopoulos, A.Z., Quirke, N., Stapleton, M. and Tildesley, D.J. (1988) "Phase equilibria by simulation in the Gibbs ensemble: alternative derivation, generalization and application to mixture and membrane equilibria", *Mol. Phys.* **63**, 527–545.

[24] Nitta, T., Nozawa, M. and Hishikawa, Y. (1993) "Monte Carlo simulation of adsorption of gases in carbonaceous slitlike pores", *J. Chem. Eng. Japan* **26**, 266–272.

[25] McGrother, S.C. and Gubbins, K.E. (1999) "Constant pressure Gibbs ensemble Monte Carlo simulations of adsorption into narrow pores", *Mol. Phys.* **97**, 955–965.

[26] Kofke, D.A. (1993) "Direct evaluation of phase coexistence by molecular simulation via integration along the saturation line", *J. Chem. Phys.* **98**, 4149–4162.

[27] Allen, M.P. and Tildesley, D.J. (1987) *Computer Simulation of Liquids* (Clarendon Press, Oxford).